Intense vortex laser generation and phase detection by surface plasma holograms: Supplementary information

Hao Zhang[1], Lingyu Zhang[1], Hongtao Huang[1], Jingyi Wang[1], Yuanjie Yang[2], Wenhui Tang[3], and Tongpu Yu[1]

[1]*Department of Physics, National University of Defense Technology, Changsha 410073, China*
[2]*School of Physics, University of Electronic Science and Technology of China, Chengdu 610056, China*
[3]*Department of Nuclear Science and Technology, National University of Defense Technology, Changsha 410073, China*

Abstract
This supplemental document comprises information of the depth distribution of surface plasma holograms (SPHs), the generation of SPHs in the cases of higher-order modes, oblique incidences of object laser, the reflected vortex laser in the case of a longer time delay of read-out laser, and hydrocarbon targets. The proposed experimental setup is included as well.

Keywords: plasma optics; relativistic vortex lasers; plasma holograms; laser-plasma interaction

After obtaining the SPH density distributions for the cases of the object laser with initial phase (a) 0, (b) $\pi/2$, (c) only having the object laser, and (d) only having the reference laser, we calculated the distance from the initial target surface position to the location where the SPHs density is approximately $1n_c$. Figures S1 show the SPHs depth distribution in four cases. As shown in the Figs. S1(a)-(b), when varying the initial phase of the object laser, the pattern of the SPHs remains unchanged but undergoes rotation.

To verify the generation of SPHs under the conditions of high-order laser modes, we carried out two simulations by changing the object laser parameter l to 2 at first. Figures S2(a)-(c) show the transverse distribution of the interference laser intensity and its transverse ponderomotive force, electron density, and proton density for the case of $l = 2$, respectively. The observed two spiral arms in Fig. S2(b) and (c) are in excellent agreement with the theoretical prediction as shown in Fig. 1(b). In order to explore the influence of the laser incident angle on the SPH formation, we assume an obliquely incident object laser at an angle of $\theta = 20^\circ$ with respect to the x-axis, with the focus spot of $w_0 = 12\lambda_0$ and the amplitude of object laser $a_o = 0.356$. Figures S2(d)-(f) show the transverse distribution of the interference laser intensity and its transverse ponderomotive force, electron density, and proton density for the case Eq. (3b), respectively. When the object laser is changed to a large focus spot with oblique incidence, the transverse distribution of the interference laser intensity changes from a spiral pattern to a fork pattern. Similarly, the electron and proton density distribution of the SPH also transforms into a fork pattern.

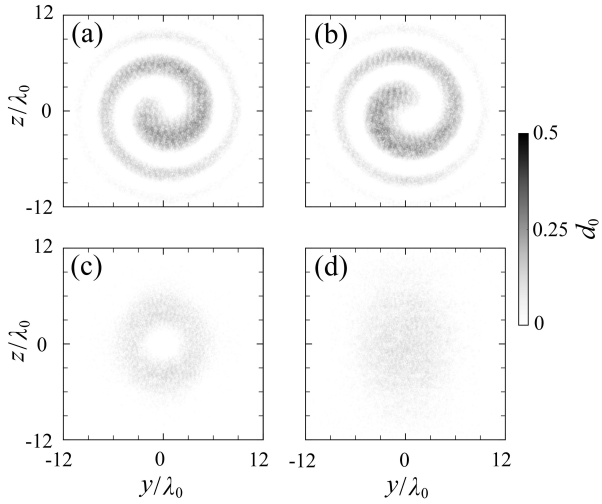

Figure 1. The distributions of the SPHs depth d_{SPH} in the case of object laser with the initial phase of 0 (a), $\pi/2$ (b), only having the object laser (c), and only having the reference laser (d), respectively.

In order to validate the applicability of this phase reconstruction method for higher-order modes and oblique

Correspondence to: T. Yu, Department of Physics, National University of Defense Technology, Changsha 410073, China, Email: tongpu@nudt.edu.cn

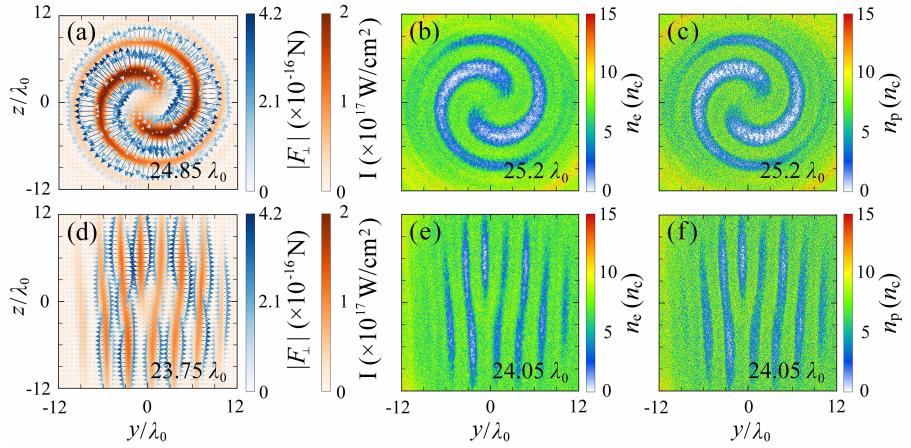

Figure 2. Transverse distribution of the interference lasers intensity and their transverse ponderomotive force at $t = 60T_0$ in the $l = 2$ case (a) and oblique incident case (d), respectively. Transverse distribution of the electron and proton density at $t = 300T_0$ in the $l = 2$ case ((b) and (c)) and oblique incident case ((e) and (f)), respectively.

incidence, we conducted theoretical calculations of the reconstructed phase and corresponding electric field distributions in these two cases. As shown in the Fig. S3(a)-(d), the theoretical results illustrate the phase and electric field distributions of the object laser for $l = 2$ modes and oblique incidence, demonstrating the robustness of this method.

We also proposed an experimental setup for realizing the vortex phase generation and detection study, as shown in Fig. S4. In experiment a primary pulse of a laser is incident from the left and is divided into two sub pulses by a spectroscope. Employing the current laboratory settings for generating relativistic vortex lasers, one of the pulse is reflected off an off-axis phase plate and is transformed into a vortex laser. The other pulse is reflected by a mirror. These two pulses are then combined into one interference laser with a beam combiner and focused onto the target by an off-axis parabolic mirror. Depending on the plasma density of the target, either visible light, near-infrared light or X-rays can be used to detect the distribution of the plasma density on the target surface[1–5].

To investigate the lifetime of surface plasmon holography, we adjusted the delay time of the laser to $320T_0$. As shown in Fig. S5, the electric field distribution of the reflected laser still maintains distinct vortex laser characteristics. This indicates that SPH has a lifetime exceeding the picosecond scale.

To investigate the effect of target material on SPH formation, we employed a hydrocarbon target. As previously discussed, SPH is formed under the ponderomotive force of the interference laser and the charge separation fields. Consequently, ions with lower charge-to-mass ratios require a longer duration of the laser for modulation. We utilized a hydrocarbon target composed of fully ionized carbon and hydrogen ions, with a density ratio of carbon to hydrogen of $1 : 4$, and the duration of object and reference pulses

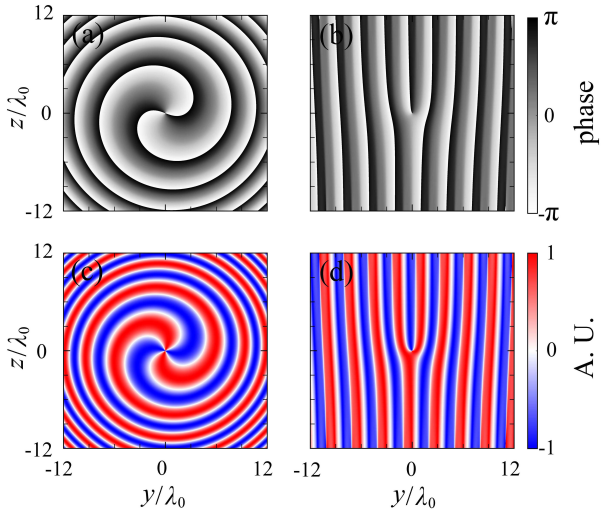

Figure 3. The reconstructed phase profiles of the object laser obtained through theoretical calculations in the $l = 2$ case (a) and oblique incident case (b), respectively. The laser electric fields obtained through theoretical calculations in the $l = 2$ case (c) and oblique incident case (d), respectively.

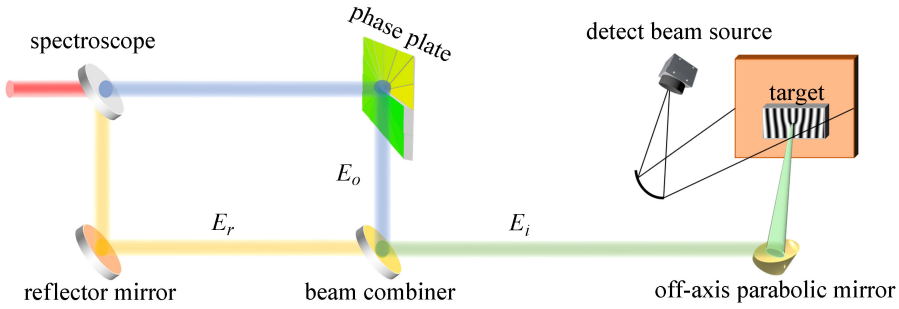

Figure 4. Proposal of an experiment set-up to acquire surface plasma hologram. A main pulse of the laser is incident from the left and is split into two sub pulses via a spectroscope. In accord with current experimental setups for generating relativistic vortex lasers, one laser pulse is reflected off an off-axis phase plate and converted into a vortex laser. The other laser pulse is reflected by a mirror. These two pulses are then combined into one interference laser pulse by a beam combiner and are focused on the target by an off-axis parabolic mirror. Depending on the plasma density of the target, visible light or X-rays can be used to detect the plasma density distribution.

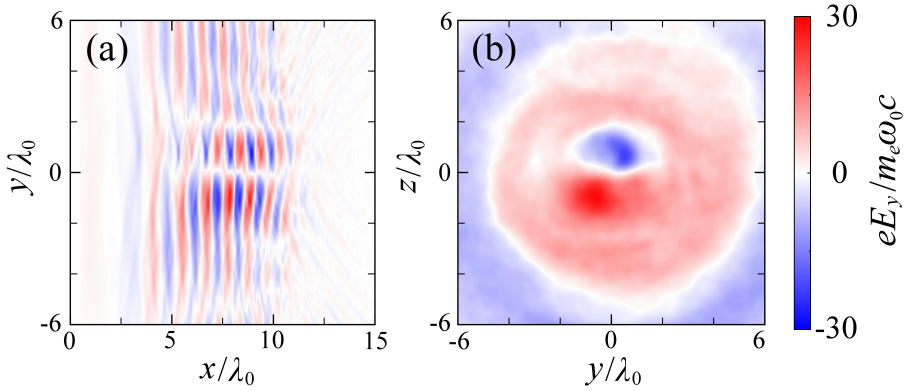

Figure 5. Distribution of electric field E_y on the (a) $x-y$ plane and (b) $y-z$ plane (at $x = 7.75\lambda_0$) and $t = 688T_0$.

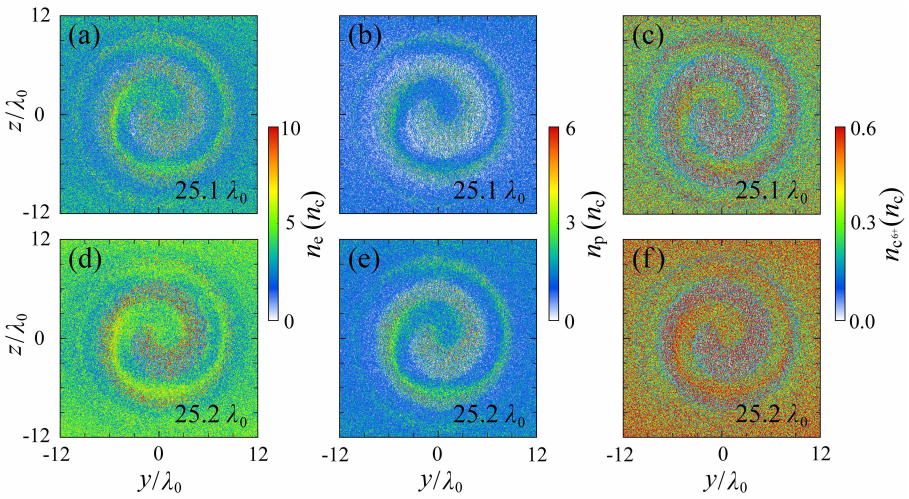

Figure 6. Transverse distribution of the electron ((a), (d)), proton ((b), (e)), and carbon ions ((c), (f)) density at $t = 720T_0$, respectively.

is $750T_0$, while keeping other parameters unchanged. As shown in Figs. S6, the density distributions of electrons, protons, and carbon ions on the target surface exhibit a helical structure consistent with that of Fig. 1(b). This indicates that the material of the target affects the formation time of SPH, but does not alter the patterns or characteristics of the SPH.

References

1. D. Ress, L. B. DaSilva, R. A. London, J. E. Trebes, S. Mrowka, R. J. Procassini, T. W. Barbee, and D. E. Lehr. Measurement of laser-plasma electron density with a soft x-ray laser deflectometer. *Science* **265**, 514–517 (1994).
2. R. Tommasini, O. L. Landen, L. Berzak Hopkins, S. P. Hatchett, D. H. Kalantar, W. W. Hsing, D. A. Alessi, S. L. Ayers, S. D. Bhandarkar, M. W. Bowers, D. K. Bradley, A. D. Conder, J. M. Di Nicola, P. Di Nicola, L. Divol, D. Fittinghoff, G. Gururangan, G. N. Hall, M. Hamamoto, D. R. Hargrove, E. P. Hartouni, J. E. Heebner, S. I. Herriot, M. R. Hermann, J. P. Holder, D. M. Holunga, D. Homoelle, C. A. Iglesias, N. Izumi, A. J. Kemp, T. Kohut, J. J. Kroll, K. LaFortune, J. K. Lawson, R. Lowe-Webb, A. J. MacKinnon, D. Martinez, N. D. Masters, M. P. Mauldin, J. Milovich, A. Nikroo, J. K. Okui, J. Park, M. Prantil, L. J. Pelz, M. Schoff, R. Sigurdsson, P. L. Volegov, S. Vonhof, T. L. Zobrist, R. J. Wallace, C. F. Walters, P. Wegner, C. Widmayer, W. H. Williams, K. Youngblood, M. J. Edwards, and M. C. Herrmann. Time-resolved fuel density profiles of the stagnation phase of indirect-drive inertial confinement implosions. *Phys. Rev. Lett.* **125**, 155003 (2020).
3. K. Dai, Q. Cui, and J. Zhang. Single-shot probing of sub-picosecond solid-to-overdense-plasma dynamics. *Light. Sci. Appl.* **13**, 162 (2024).
4. K. L. Baker. Tomographic reconstruction of high-energy-density plasmas with picosecond temporal resolution. *Opt. Lett.* **31**, 730–732 (2006).
5. D. G. Jang, M. S. Kim, I. H. Nam, H. S. Uhm, and H. Suk. Density evolution measurement of hydrogen plasma in capillary discharge by spectroscopy and interferometry methods. *Appl. Phys. Lett.* **99**, 141502 (2011).